

Polydirectional Microvibration Energy Collection for Self-Powered Multifunctional Systems Based on Hybridized Nanogenerators

Hongmei Yang, Mingming Deng, Qixuan Zeng, Xuemei Zhang, Jie Hu, Qian Tang, Huake Yang, Chenguo Hu, Yi Xi,* and Zhong Lin Wang*



Cite This: *ACS Nano* 2020, 14, 3328–3336



Read Online

ACCESS |

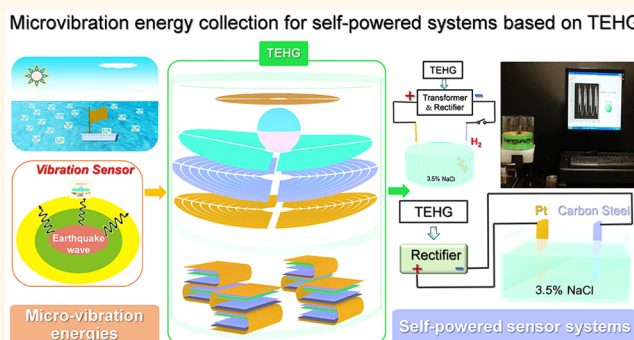
Metrics & More

Article Recommendations

Supporting Information

ABSTRACT: Vibrations in the environment are usually distributed over a wide frequency spectrum in multiple directions and a weaker amplitude, which makes most of the current vibrational energy collectors limited in practical environmental applications. Herein, a triboelectric-electromagnetic hybridized nanogenerator (TEHG) for low-frequency random microvibrational energy harvesting in all directions and a wide working bandwidth is fabricated. The output peak power of a triboelectric nanogenerator (TENG) up to 3.65 mW is realized ($\theta = 0.4$ rad, $f = 1$ Hz). In addition, a real self-powered seawater splitting system and electrochemical cathodic protection system are fabricated, directly converting blue energy to hydrogen energy, and the ships can achieve self-protection against corrosion. Furthermore, relying on the linear relationship between the number of peaks and the amplitude of vibration, a highly sensitive self-powered vibration amplitude sensor system based on LabVIEW software is achieved, which can be used as an amplitude detection of bridges and earthquake monitoring, etc. This work is an important development for harvesting low-frequency random multiple direction microvibrational energy over a wide working bandwidth and the bright future of blue energy. In addition, it has been successfully applied to the power supply of portable electronic equipment, environmental monitors, and self-powered systems.

KEYWORDS: polydirectional microvibration energy, triboelectric nanogenerators, electromagnetic generator, energy harvesting, self-powered multifunctional systems



As one of the most common mechanical energies, vibration can be seen everywhere in life, such as moving vehicles, vibrating bridges, ocean wave oscillations, etc. It has the characteristics of wide frequency spectrum, uncertain vibration direction, and random vibration form.¹ Various vibrational energy harvesters have been designed by relying on piezoelectric,^{2–4} electromagnetic,^{5,6} and electrostatic^{7,8} transmission principles. Recently, the newly invented triboelectric nanogenerator (TENG), relying on contact electrification and electrostatic induction, has been regarded as an advanced invention for random and low-frequency vibrational energy harvesting with the merits of light weight, low price, simple structure, high power density, and high conversion efficiency.^{9–11} Multifarious TENGs for vibrational energy harvesting have been fabricated.^{12–18} However, most of them can only obtain vibration energy effectively from one direction or within a small bandwidth, or vibration energy can only be collected at large amplitudes,

resulting in a limitation in practical environmental application because the natural vibration frequency of the environment is usually lower than 50 Hz and the amplitude of the ambient vibration is relatively weak.^{19,20} How to harvest those microvibrational mechanical energies with multidirection and a wide working bandwidth is the main barrier. Furthermore, for most of the self-powered systems based on TENGs, the energy supply component and the application part are separated,^{21–27} designing a special structure and integrating the two parts into one is the crux of realizing a real self-powered system.

Received: November 13, 2019

Accepted: February 12, 2020

Published: February 12, 2020

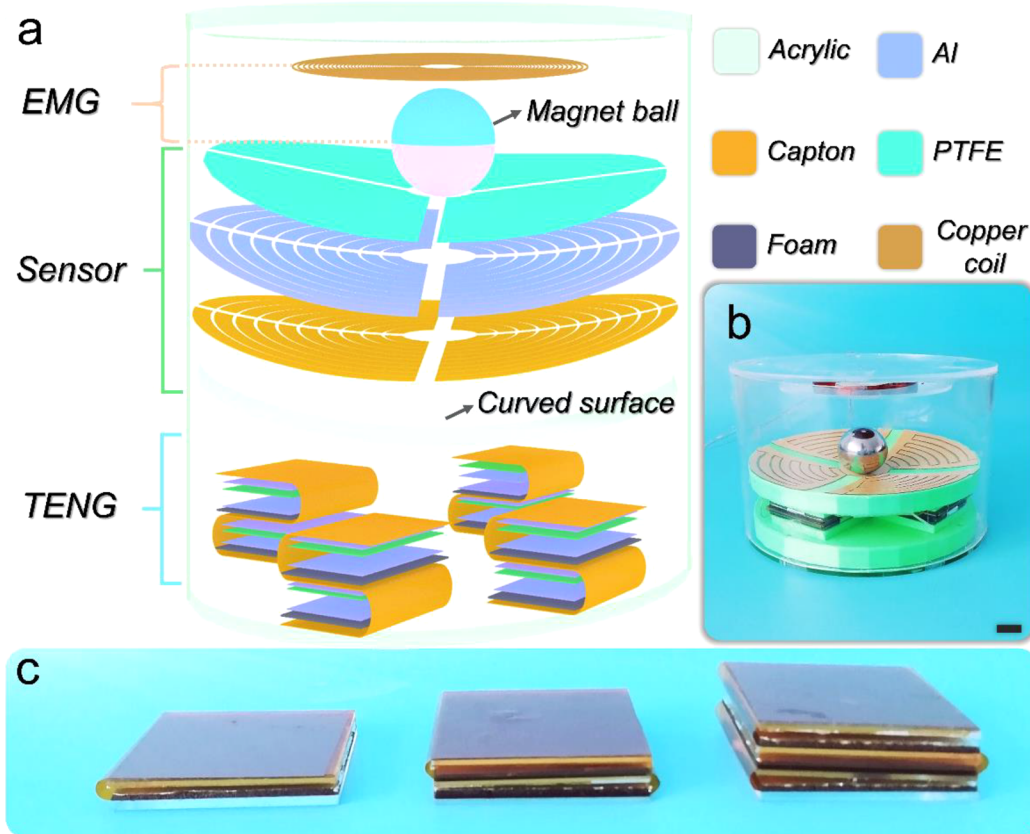


Figure 1. Structural design of the TEHG. (a) Schematic diagram of TEHG, which mainly consists of three parts: a single EMG unit, a self-powered vibration amplitude sensor, and four zigzag multilayered TENGs units. (b) Photograph of the fabricated TEHG; the scale bar is 15 mm. (c) Photograph of multilayered TENGs from one to three layers.

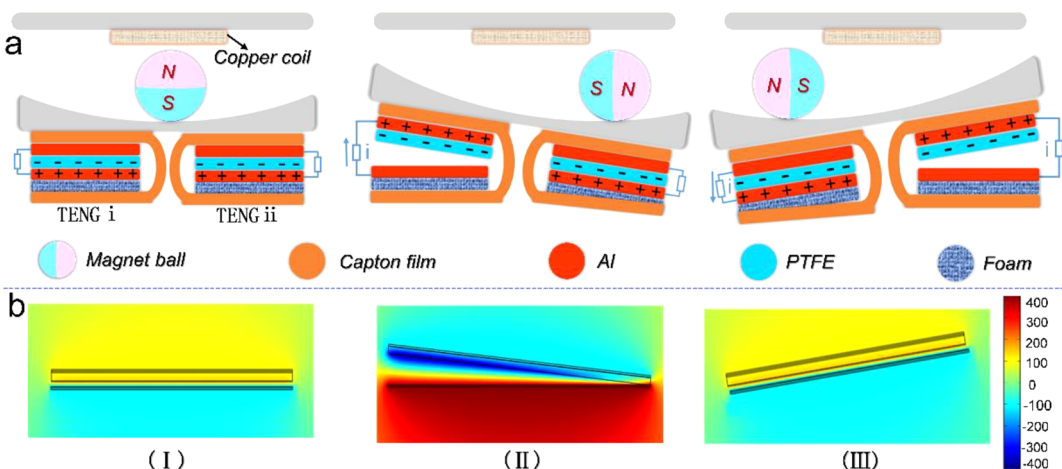


Figure 2. Schematics of operating principle of the hybridized generator. (a) Schematic illustrations of working mechanism and charge distribution of TENG. (b) Potential distribution by COMSOL was employed to elucidate the working principle of TENGi: (I) the initial state; (II) the intermediate state; (III) the final state.

In this work, we fabricate a triboelectric–electromagnetic hybridized nanogenerator (TEHG) including a single electromagnetic generator (EMG) unit, a self-powered vibration amplitude sensor, and four zigzag multilayered TENG units. Here, the magnet ball serves as the magnetic source for EMG, positive friction material for vibration amplitude sensor, and the trigger for multilayered TENGs simultaneously. The three parts are mainly connected by a 3D-printed circular curved surface in the middle, making the magnet ball able to reach

more active area under a small waggle and roll in all directions.²⁸ Testing result indicates that the output peak powers of TENG is 3.65 mW when the amplitude of vibration (θ) is 0.4 rad, working frequency is 1 Hz, revealing superior advantages of collecting low-frequency microvibration energy. In addition, this hybrid generator is promising to be used in blue energy harvesting from rough seas to calm seas, especially for the calm seas, which is more common in real oceans.²⁸ A self-powered seawater splitting system and a self-powered

electrochemical cathodic protection system are fabricated with the collected blue energies from a minor water wave, which realizes a direct conversion from blue energy to hydrogen energy, and the ships can achieve self-protection against corrosion by this device. Furthermore, relying on the linear relationship between the number of peaks and the amplitude of vibration, a highly sensitive self-powered vibration amplitude sensor system is achieved, which can be used as an amplitude detection for bridges and earthquake monitoring, etc. This hybridized nanogenerator is an important step of harvesting low-frequency random multiple direction microvibrational energy over a wide working bandwidth and the bright future of blue energy. In addition, it has been successfully applied to the power supply of portable electronic equipment, environmental monitors, and self-powered systems.

RESULTS AND DISCUSSION

Structural Design. The structure of the TEHG is presented in Figure 1a, which mainly consists of three contents: a single EMG unit, a self-powered vibration amplitude sensor, and four zigzag multilayered TENG units. Here, the magnet ball serves as a magnetic source for EMG, a positive friction material for vibration amplitude sensor, and the trigger for multilayered TENGs simultaneously. The three parts are mainly connected by a 3D-printed circular curved surface in the middle, making the magnet ball able to reach more active areas under a small waggle and roll in all directions. Relative rotation between the magnet ball and circular curved surface occurs as the device is vibrated arbitrarily under an external force, causing periodic trigger of three parts. Figure 1b,c shows the photographs of TEHG (the scale bar is 15 mm) and the multilayered TENGs from one to three layers, respectively.

Schematics of Operating Principle. Figure 2 is the working mechanism of TEHG for microvibration energy harvesting, which can be regarded as three successive procedures in a complete circle. Figure 2a is a schematic illustration of the working mechanism and charge distribution of two contact-separation mode TENG units. When the two different dielectric materials come into contact with each other by the pressure of the magnet ball, there will be equal amounts of triboelectric charges on the two dielectric material surfaces based on the triboelectrification effect. An electric potential drop between the two electrodes will be built as long as the two dielectric materials are separated by the rolling of the magnet ball. In order to achieve static balance, the electrons will be driven to flow between the two electrodes because of the electrostatic induction.^{10,29} Furthermore, the voltage between the two electrodes can be expressed by this formula:^{30,31}

$$V = \frac{\sigma_1(z, t)d_1}{\epsilon_1} + \frac{[\sigma_1(z, t) - \sigma_c]z(t)}{\epsilon_0} \quad (1)$$

where $\sigma_1(z, t)$ is the charge density cumulated by free electrons, d_1 is the dielectric thickness, σ_c is the saturated charge density on the surface of dielectric 1, $z(t)$ is the distance between dielectric layer and electrode, and ϵ_0 and ϵ_1 are dielectric constants of air and dielectrics, respectively. For conductor-to-dielectric CS-TENG, with no charge transfer in the open circuit, the open-circuit voltage V_{oc} is represented by³²

$$V_{oc} = \frac{\sigma_c z(t)}{\epsilon_0} \quad (2)$$

In the case of the short circuit, the voltage is 0. So the transferred charges and short-circuit I_{sc} current can be given by the following formulas:

$$Q_{sc} = \frac{S\sigma_c z(t)}{d_0 + z(t)} \quad (3)$$

$$I_{sc} = \frac{dQ_{sc}}{dt} = \frac{S\sigma_c d_0 V(t)}{(d_0 + z(t))^2} \quad (4)$$

where $d_0 = d_1/\epsilon_1$, S is the contact area, and $V(t)$ is the contact-separation speed between the two dielectric materials, respectively. Figure 2b illustrates the electric potential variation between two aluminum electrodes of TENGi simulated by COMSOL software. These results indicate that multilayered zigzag TENG units and variable magnetic flux in copper coil can be periodically triggered by this device to convert the microvibration energies into electricity. Therefore, this device can be used as the microvibration energy harvester, such as water wave, vibration of ships, vehicles, and bridges or any other vibrating objects that can integrate this device.

Electric Output Performance. To investigate the features of the hybridized generator for harvesting microvibration energies, the influence of different parameters on the output performance of one-layer TENG has been systematically tested, e.g., the distance of contact separation (d_{c-s}), the thickness of Capton film (T_{Capton}), curvature of the circular curved surface (ρ), the diameter of the magnet ball (d_{ball}), contact area (s), etc., and the results are displayed in Figure S1. It can be seen that the Capton film with d_{c-s} is 3 cm (Figure S1a), and T_{Capton} at 0.05 mm (Figure S1b) can obtain the optimal output. From eq 2, we can conclude that the open-circuit voltage (V_{oc}) is in proportion to $z(t)$ (equivalent to d_{c-s}), but when d_{c-s} is 4 cm, the output is less than that at 3 cm (Figure S1a). It can be contributed to the fact that the Capton film based TENG can be considered as a spring oscillator; Capton films with different d_{c-s} and thicknesses correspond to different k and X from Hooke's law, $F = kX$ (here, X is the distance between contact and separation of TENG, which is closely related to d_{c-s} and k is the equivalent spring stiffness coefficient). The optimal output can be acquired under the same driving force only with the appropriate stiffness coefficient. Then, the circular curved surface with ρ at 200 mm and d_{ball} at 50 mm is used to explore the relationship between V_{oc} and the amplitude of vibration (θ), as shown in the Figure S1c (left part is the schematic illustration of radian of vibration). It indicates that when θ is 0.4 rad, the magnet ball can roll to the edge of the circular curved surface and obtain maximum rolling distance, resulting in a maximum d_{c-s} of the TENG, obtaining a maximum output with 350 V. In addition, voltage versus ρ and d_{ball} in Figure S1d manifests that when θ is 0.13 rad, the output voltage is positively correlated with ρ and d_{ball} . The reason is that when θ is 0.13 rad, the magnet ball cannot roll to the edge of the circular curved surface. So the bigger the d_{ball} , the greater the pressure on TENG, and a fuller contact can be obtained. With the larger the ρ , the farther the ball rolls, resulting in a bigger d_{c-s} , therefore obtaining a larger voltage. These results suggest that this device has its advantages and potential application value in collecting random microvibrational energy in multiple

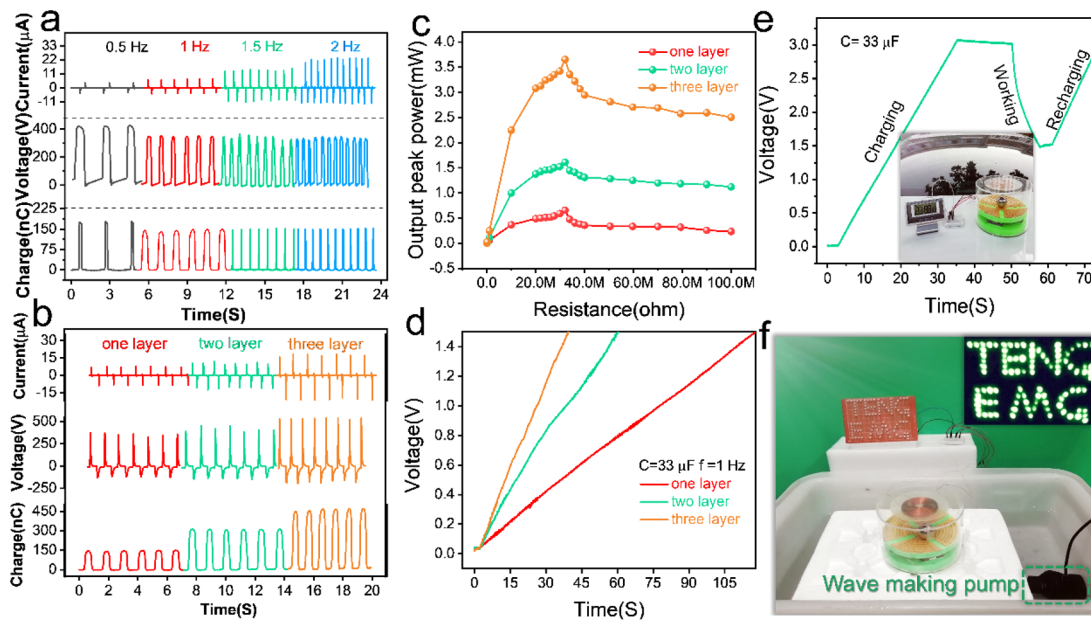


Figure 3. Electrical output performance of zigzag multilayered TENG. (a) Short-circuit current (I_{sc}), open-circuit voltage (V_{oc}), transfer charge of one layered TENG unit on working frequency ranging from 0.5 to 2 Hz. (b) I_{sc} , V_{oc} (the logic testing circuit is shown as Figure S4a), and transfer charge of different layered TENGs. (c) Average power vs resistance of external load and (d) measured voltages of a $33 \mu\text{F}$ capacitor charged by different layered TENGs. (e) Measured voltages of a $33 \mu\text{F}$ capacitor charged by TENG parts as the power source of a digital watch. The inset photograph is schematic diagram of collecting vibration energy from a car. (f) Demonstrations for collecting minor water wave energy as the power source of LEDs.

directions, and it can be adapted to various application scenes of microvibration by adjusting the curvature of the circular curved surface. As is well-known, the contact area has a great influence on the output characteristics of TENG according to eqs 3 and 4, Figure S1e shows that the charge density of TENG with smaller size ($2 \text{ cm} \times 2 \text{ cm}$) is 2.8 times higher than that of TENG with larger size ($5 \text{ cm} \times 5 \text{ cm}$), which was due to the enhanced contact effectivity with small dimension. Herein, the hybridized nanogenerator for harvesting micro-vibration energies is fabricated with above optimal parameters ($d_{c-s} = 3 \text{ cm}$, $T_{\text{Capton}} = 0.05 \text{ mm}$, $\rho = 200 \text{ mm}$, $s = 16 \text{ cm}^2$).

The electrical output characterization of the hybrid generator was quantitatively investigated with a microstep driver in Figure 3 and Figures S2 and S3. The short-circuit current (I_{sc}), open-circuit voltage (V_{oc}), and transfer charge dependence on frequency (0.5 to 2 Hz) of one-layered TENG in Figure 3a indicates that as current is the amount of charge transferred per unit time, it is positively related to working frequency; I_{sc} increases gradually from 4 to $23.5 \mu\text{A}$. In contrast, V_{oc} gradually decreases from 420 to 350 V because σ_c decreased with the increase of frequency due to insufficient contact, which is consistent with the change trend of transfer charge (decrease from 175.3 to 152.6 nC). The output performances of different layered TENGs (layers are connected in parallel) are shown in Figure 3b,c. Those two figures indicate that I_{sc} (increases from 7.3 to $18.9 \mu\text{A}$), V_{oc} (increases from 376 to 541.7 V ; the logic testing circuit is shown as Figure S4a), transfer charge (increases from 155.6 to 477.3 nC), and output peak power (increases from 0.65 to 3.65 mW obtained at $32 \text{ M}\Omega$) of different layered TENGs can be superimposed, indicating that more layers can obtain bigger output. A comparison table (Table S1) of the output performance of TEHG with the other devices already reported also suggests that this device has the excellent output performance even though at such lower working frequency.

^{13,33–36} Figure 3d shows the voltages of a $33 \mu\text{F}$ capacitor charged by different zigzag multilayered TENGs (the circuit diagrams are in Figure S4b); the capacitor can be charged to 1.5 V in 39 s with three layered TENGs and Figure 3e (four units) shows that this device can be used as the power source of a digital watch. The inset is the schematic diagram of collecting vibration energy from a car. Those data were obtained at $\theta = 0.4 \text{ rad}$, $f = 1 \text{ Hz}$. Figure 3f indicates that the minor water wave energy can be changed to electricity by this device as the power source for electronics, such as LEDs, as shown in Supporting Information Movie S1, revealing the potential of application in blue energy from rough seas to calm seas, especially for the calm seas, which is more common in real oceans. The rectified I_{sc} of the TENG part with four units driven by minor water wave is shown in Figure S2a with stable output about $14.5 \mu\text{A}$.

In addition, the reliability of the device must be considered in practical applications. Figure S2b shows the rectified I_{sc} of the TENG before and after 500k cycles of continuous work. After a long time of continuous work, no obvious current attenuation was found, which indicates that the device has excellent mechanical durability. Furthermore, for blue energy harvesting, the effect of humidity and salinity on the output should be discussed, and the 3.5 wt % NaCl solution was used to simulate ocean salinity conditions. It can be concluded that salinity has no effect on output voltage according to Figure S2c (the relative humidity is 87%), and there is no obvious normalized voltage decay in Figure S2d with different humidity (from 37 to 94%), which shows that the full-packaged structure isolated the effect of the chloride ion and water molecule on the surface of friction materials effectively.³⁷

Figure S3 illustrates the electrical output performance of the EMG. The performances driven by a water wave can obtain a stable electric output with $I_{sc} \sim 23 \text{ mA}$ and $V_{oc} \sim 10 \text{ V}$, respectively (Figure S3a), and the $100 \mu\text{F}$ capacitor can be

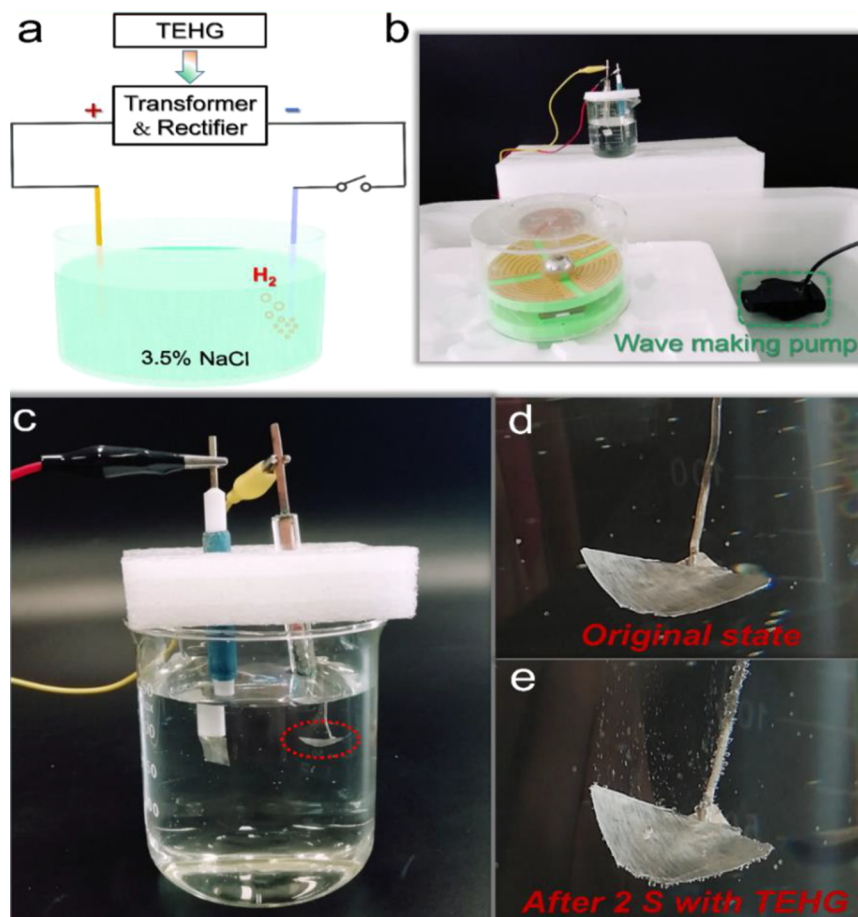


Figure 4. Self-powered seawater splitting system (3.5 wt % NaCl solution is used in place of seawater). (a) Schematic diagram, (b,c) photographs of the TEHG-driven water splitting system. (d,e) Enlarged view in (c) of the Pt plate.

charged to 9.57 V within 4.25 s (Figure S3b). In addition, the relationship between output performance and radian of vibration in Figure S3c shows that when θ exceeds 0.4 rad, the maximum variable magnetic flux can be obtained with $I_{sc} \sim 22.9$ mA and $V_{oc} \sim 10.1$ V. Figure S3d suggests that when the external load is $350\ \Omega$, the peak power can be obtained with 22.4 mW at 1 Hz, $\theta = 0.4$ rad. It is well-known that a TENG is more efficient for low-frequency (<2 Hz) energy harvesting whereas an EMG has the opposite effect according to Faraday's law of electromagnetic induction. Hence, the working frequency ranges can be broadened with this triboelectric–electromagnetic hybrid structure, and those microvibrational mechanical energies with a wide working bandwidth can be harvested effectively.

Self-Powered Seawater Splitting System. Those above results suggest that this hybrid generator can convert the microvibration energy into electricity effectively, and we show that it can be directly used for a self-powered seawater splitting system. Figure 4a is a diagram showing the self-powered splitting of seawater into H_2 . Here, 3.5 wt % NaCl solution is used in place of seawater for improving the conductivity, and a Pt plate is used as the electrode. The mechanism is as follows through the electrolysis effect:³⁸

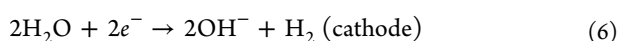
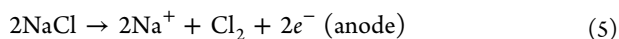


Figure 4b,c shows the pictures of the fabricated self-powered water splitting system, and the minor water wave energy can be harvested as the power source of the water splitting system after being transformed and rectified. The enlarged view of the Pt electrode in Figure 4c is illustrated as Figure 4d,e; it can be seen that the Pt electrode produces a large number of hydrogen bubbles after 2 s with TEHG, and the dynamic splitting process can be found in Supporting Information Movie S2, indicating that the blue energy can be directly converted to hydrogen energy by this device. In practical application, hydrogen can be collected and utilized by a drainage method to realize a self-powered and pollution-free clean energy production system, which has great application potential in production and life.

Self-Powered Electrochemical Cathodic Protection System. In addition, according to the cathodic protection effect, this device can also be used as a power source for protecting metals from corrosion. Figure 5a shows the illustration of the self-powered electrochemical cathodic protection system. The positive pole of the rectifier is connected to the Pt electrode, and the negative pole is connected to the carbon steel. Therefore, the electrons generated by the TEHG would be poured onto the carbon steel surface to limit corrosion.²¹ The open-circuit potential (OCP) drop is used to estimate the efficiency of cathodic protection in a cathodic protection system. Generally, the greater the negative shift of OCP, the better the effect of cathodic protection.³⁹ In the three-electrode system, the

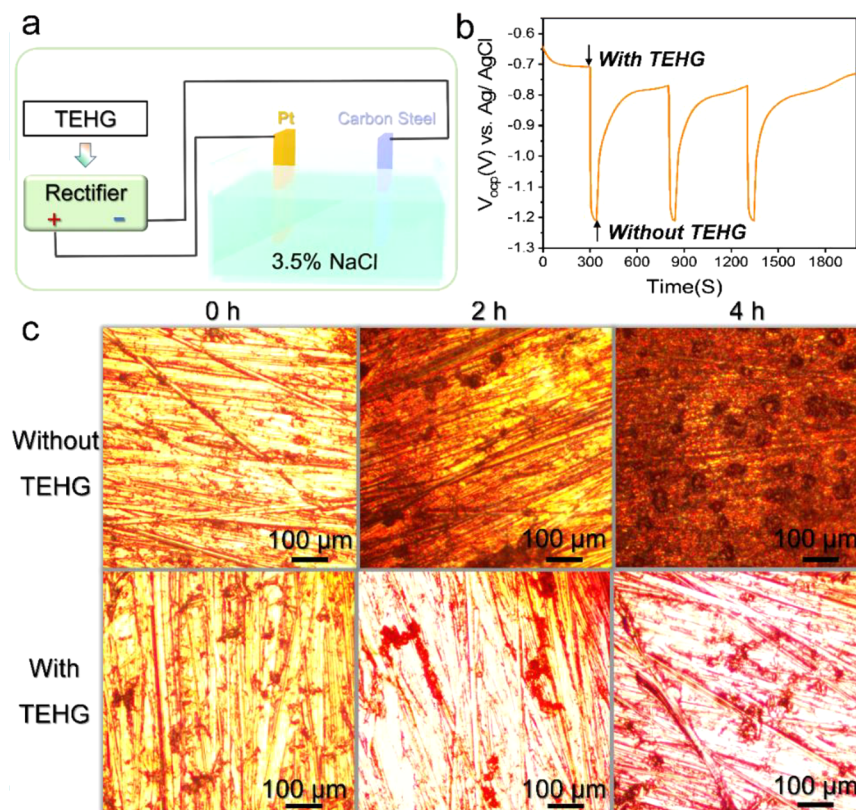


Figure 5. Self-powered electrochemical cathodic protection system. (a) Schematic diagram of Q235 carbon steel cathodic protection in 3.5 wt % NaCl solution. (b) OCP changes of Q235 carbon steel coupled with and without TEHG. (c) Microscopy images of the Q235 carbon steel immersed in 3.5 wt % NaCl solution for 0, 2, and 4 h, separately connected without (the top views) and with TEHG (the bottom views).

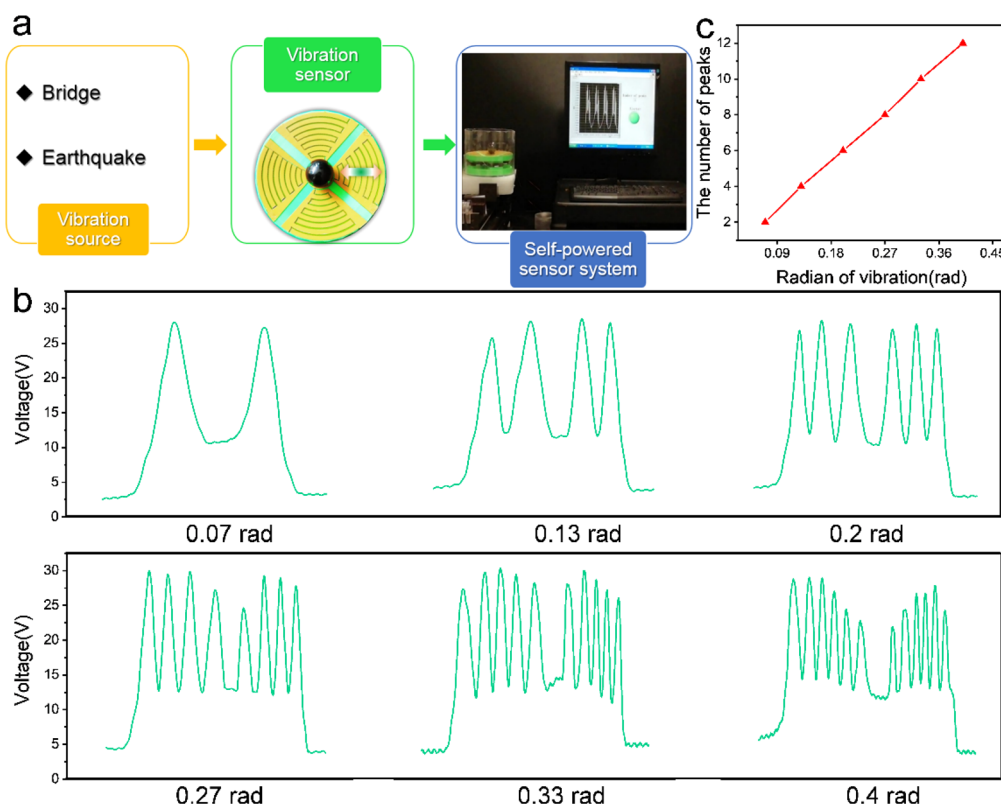


Figure 6. Self-powered vibration amplitude sensor system. (a) Illustration of self-powered vibration amplitude sensor system based on LabVIEW software. (b) Output voltage with different radian. (c) Relationship between peak number and radian of vibration.

change of OCP in carbon steel with and without TEHG was measured with Pt as the counter electrode and Ag/AgCl as the reference electrode in 3.5 wt % NaCl solution, as shown in **Figure 5b**. The OCP without TEHG is about -0.7 V (*vs* Ag/AgCl) and shifts to -1.2 V (*vs* Ag/AgCl) after powering by the TEHG. Hence, the negative shift of OCP is about 500 MV, indicating that the carbon steel is effectively cathodically protected. The periodic change of the OCP suggests the high availability of TEHG as the power source of the cathodic protection system.

The microscopy images in **Figure 5c** are used to observe the efficiency of cathodic protection, and the carbon steels after being polished were immersed into 3.5 wt % NaCl solution from 0 to 4 h. The results show that the carbon steel surface is completely covered by red rust after being soaked for 2 h, and the degree of corrosion becomes worse with the increase of soaking time. However, there is only a minor traces of corrosion after being soaked for 4 h with TEHG. Therefore, the cathodic protection system with TEHG is an effective method of electrochemical corrosion protection, which has great application value in self-powered anticorrosion protection of ships when this device is integrated on it.

Self-Powered Vibration Amplitude Sensor System.

Figure S1c,d suggests that the rolling distance of the magnet ball is closely related to θ , ρ , and d_{ball} . Therefore, it can be used as a vibration amplitude sensor when ρ and d_{ball} are constant, as shown in **Figure 6**. Different rolling distances of the magnet ball with different amplitude of vibration (θ) correspond to different number of signals, as shown in **Figure 6b**. The point-line diagram in **Figure 6c** indicates that there is almost linear correlation between the number of peaks and the amplitude of vibration, and the functional relationships can be expressed as

$$Y = 33.33\theta + 0.33 \quad (7)$$

where Y is the number of signals and θ is the amplitude of vibration. In order to exhibit the ability of online supervision, a self-powered amplitude of the vibration monitoring system based on LabVIEW software is fabricated shown, as **Figure 6a**. Here, a flabellate free-standing mode TENG was used to capture the signal of vibration amplitude, and the working mechanism is shown in **Figure S5** (magnet ball acts as the positive friction material). A linear motor is used to produce a sustained and stable oscillation; the alertor can be awakened successfully every time when the vibration amplitude reaches the preset value, and the dynamic process is displayed in **Supporting Information Movie S3**, suggesting that the high sensitivity of the sensor and the sensitivity can be improved by reducing the width of the electrode. Moreover, it also has the potential application in self-powered direction sensing of the vibration source, and the sensitivity can be adjusted by changing the number of segments in the sector. Those results illustrate that this self-powered vibration amplitude sensor system can be used as the amplitude detection of bridges and earthquake monitoring, etc., as long as the relationship between vibration characteristics and number of signals is defined.

CONCLUSIONS

We have designed a triboelectric–electromagnetic hybridized nanogenerator for low-frequency random microvibrational energy harvesting in multiple directions and a wide working bandwidth. In addition, this hybridized generator is promising to be used in blue energy harvesting from rough seas to calm seas, especially for the calm seas, which is more common in the

real oceans. Furthermore, the special structure design renders the energy supply component and the application part into one, and a real self-powered seawater splitting system, electrochemical cathodic protection system, and a highly sensitive vibration amplitude sensor system have been achieved. This work is an important step for harvesting low-frequency random microvibrational energy from all directions as well as the bright future of blue energy. In addition, it has been successfully applied to the power supply of portable electronic equipment, environmental monitors, and self-powered systems.

EXPERIMENTAL SECTION

Fabrication of Three-Layered TENG. First, the Kapton film was cut into a rectangle (length (L) 12.9 cm, thickness (T) 0.05 mm, width (W) 4 cm). Then, the Kapton film was folded into a zigzag shape. Foam rubber ($T = 1$ cm) covered with aluminum film ($T = 0.01$ mm) was stuck to one side of the Kapton film of every layer as one tribolayer and electrode. Next, the same size aluminum ($T = 0.01$ mm) film and PTFE film (T 0.05 mm) were pasted on the other side of the Kapton film of every layer as another electrode and tribolayer, respectively. The basic CS-TENG unit was fabricated successfully, as shown in **Figure 1a** for the TENG part. Finally, one side of the multilayered zigzag TENG was fixed to the upper surface of the bottom 3D-printed disc, and the other side was fixed to the lower surface of the top 3D-printed circular curved surface (the bottom of the circular curved surface is flat).

Fabrication of EMG. First, the copper coil (1500 laps with 0.018 mm diameter of copper wire) was installed on the bottom of acrylic disc cut by a laser cutter. Then, one magnet ball with the diameter 3 cm was placed on the surface of the circular curved surface. The two parts worked as the EMG part in **Figure 1a**.

Fabrication of Vibration Amplitude Sensor. The vibration amplitude sensor was designed as the quartering flabellate structure, and a free-standing mode TENG was adopted with an aluminum interdigital electrode. The width of the electrode was 5 mm, and the space between electrodes was 1 mm. Here, PTFE film (T :0.05 mm) was used as negative tribolayer, and the magnet ball acted as the positive tribolayer and the trigger of the sensor. When the magnet ball rolls by external force, the number and the source of the signal reflects the amplitude and direction of vibration.

Measurement and Characterization. A Keithley 6514 system electrometer based on LabVIEW software platform was used to measure the output performances of the device. A finite-element simulation relying on Comsol Multiphysics software was used to calculate the potential distribution of the TENG. The output of the device was quantitatively investigated with a Microstep driver (MA860H). The water wave was simulated by a wave making pump. A linear motor (42HBS48BJ4-TR0) was used to produce a sustained and stable oscillation for the vibration sensor system. An optical microscope (Olympus IX73) was used to observe the degree of corrosion of the carbon steel. The OCP variation was tested with an electrochemical workstation (CHI 660E) in a three-electrode system, and the reference electrode was Ag/AgCl and the counter electrode was a Pt plate.

ASSOCIATED CONTENT

SI Supporting Information

The Supporting Information is available free of charge at <https://pubs.acs.org/doi/10.1021/acsnano.9b08998>.

Figures show the optimization of one layered TENG, electric output performance of TENG and EMG, schematic diagram of logic circuit and the schematic illustrations of working mechanism and charge distribution of the amplitude of vibration sensor, and a

comparison table of the output performance of TEHG with the other devices already reported ([PDF](#))

Movie 1 shows LED arrays powered by the device by minor water wave ([AVI](#))

Movie 2 shows a self-powered seawater splitting system ([AVI](#))

Movie 3 shows a self-powered vibration amplitude sensor system based on LabVIEW software ([AVI](#))

AUTHOR INFORMATION

Corresponding Authors

Yi Xi — *State Key Laboratory of Power Transmission Equipment & System Security and New Technology, Department of Applied Physics, School of Chemistry and Chemical Engineering, Chongqing University, Chongqing 400044, China; [orcid.org/0000-0002-7559-8364](#); Email: xi6@cqu.edu.cn*

Zhong Lin Wang — *Beijing Institute of Nanoenergy and Nanosystems, Chinese Academy of Sciences, Beijing 100083, China; [orcid.org/0000-0002-5530-0380](#); Email: zhong.wang@mse.gatech.edu*

Authors

Hongmei Yang — *State Key Laboratory of Power Transmission Equipment & System Security and New Technology, Department of Applied Physics, School of Chemistry and Chemical Engineering, Chongqing University, Chongqing 400044, China*

Mingming Deng — *State Key Laboratory of Power Transmission Equipment & System Security and New Technology, Department of Applied Physics, School of Chemistry and Chemical Engineering, Chongqing University, Chongqing 400044, China*

Qixuan Zeng — *State Key Laboratory of Power Transmission Equipment & System Security and New Technology, Department of Applied Physics, School of Chemistry and Chemical Engineering, Chongqing University, Chongqing 400044, China*

Xuemei Zhang — *State Key Laboratory of Power Transmission Equipment & System Security and New Technology, Department of Applied Physics, School of Chemistry and Chemical Engineering, Chongqing University, Chongqing 400044, China*

Jie Hu — *State Key Laboratory of Power Transmission Equipment & System Security and New Technology, Department of Applied Physics, School of Chemistry and Chemical Engineering, Chongqing University, Chongqing 400044, China*

Qian Tang — *State Key Laboratory of Power Transmission Equipment & System Security and New Technology, Department of Applied Physics, School of Chemistry and Chemical Engineering, Chongqing University, Chongqing 400044, China*

Huake Yang — *State Key Laboratory of Power Transmission Equipment & System Security and New Technology, Department of Applied Physics, School of Chemistry and Chemical Engineering, Chongqing University, Chongqing 400044, China*

Chenguo Hu — *State Key Laboratory of Power Transmission Equipment & System Security and New Technology, Department of Applied Physics, School of Chemistry and Chemical Engineering, Chongqing University, Chongqing 400044, China; [orcid.org/0000-0002-3019-493X](#)*

Complete contact information is available at:
<https://pubs.acs.org/10.1021/acsnano.9b08998>

Author Contributions

H.Y. and M.D. contributed equally to this work.

Notes

The authors declare no competing financial interest.

ACKNOWLEDGMENTS

This work is supported by the National Key R&D Project from Minister of Science and Technology (2016YFA0202704), NSFC (51772036), NSFCQ (cstc2019jcyj-msxmX0068), the Fundamental Research Funds for the Central Universities (2019CDXZWL001, CYFH201822), and Analytical and Testing Center of Chongqing University for TEM, SEM, and XRD.

REFERENCES

- (1) Wang, Z. L. Self-Powered Nanotech - Nanosize Machines Need Still Tinier Power Plants. *Sci. Am.* **2008**, *298*, 82–87.
- (2) Qin, Y.; Wang, X.; Wang, Z. L. Microfibre-Nanowire Hybrid Structure for Energy Scavenging. *Nature* **2008**, *451*, 809–813.
- (3) Wang, Z. L.; Song, J. Piezoelectric Nanogenerators Based on Zinc Oxide Nanowire Arrays. *Science* **2006**, *312*, 242–246.
- (4) Zeng, W.; Tao, X.-M.; Chen, S.; Shang, S.; Chan, H. L. W.; Choy, S. H. Highly Durable All-Fiber Nanogenerator for Mechanical Energy Harvesting. *Energy Environ. Sci.* **2013**, *6*, 2631–2638.
- (5) Kwon, S.-D.; Park, J.; Law, K. Electromagnetic Energy Harvester with Repulsively Stacked Multilayer Magnets for Low Frequency Vibrations. *Smart Mater. Struct.* **2013**, *22*, No. 055007.
- (6) Wang, X. Y.; Palagummi, S.; Liu, L.; Yuan, F. G. A Magnetically Levitated Vibration Energy Harvester. *Smart Mater. Struct.* **2013**, *22*, No. 055016.
- (7) Beeby, S. P.; Torah, R. N.; Tudor, M. J.; Glynne-Jones, P.; O'Donnell, T.; Saha, C. R.; Roy, S. A Micro Electromagnetic Generator for Vibration Energy Harvesting. *J. Micromech. Microeng.* **2007**, *17*, 1257–1265.
- (8) Sari, I.; Balkan, T.; Kulah, H. An Electromagnetic Micro Power Generator for Wideband Environmental Vibrations. *Sens. Actuators, A* **2008**, *145*, 405–413.
- (9) Fan, F.-R.; Tian, Z.-Q.; Lin Wang, Z. Flexible Triboelectric Generator. *Nano Energy* **2012**, *1*, 328–334.
- (10) Wang, Z. L.; Jiang, T.; Xu, L. Toward the Blue Energy Dream by Triboelectric Nanogenerator Networks. *Nano Energy* **2017**, *39*, 9–23.
- (11) Zi, Y.; Guo, H.; Wen, Z.; Yeh, M. H.; Hu, C.; Wang, Z. L. Harvesting Low-Frequency (<5 Hz) Irregular Mechanical Energy: A Possible Killer Application of Triboelectric Nanogenerator. *ACS Nano* **2016**, *10*, 4797–4805.
- (12) Zhong, W.; Xu, L.; Yang, X.; Tang, W.; Shao, J.; Chen, B.; Wang, Z. Open-Book-Like Triboelectric Nanogenerators Based on Low-Frequency Roll-Swing Oscillator for Wave Energy Harvesting. *Nanoscale* **2019**, *11*, 7199–7208.
- (13) Hu, Y.; Yang, J.; Jing, Q.; Niu, S.; Wu, W.; Wang, Z. L. Triboelectric Nanogenerator Built on Suspended 3D Spiral Structure as Vibration and Positioning Sensor and Wave Energy Harvester. *ACS Nano* **2013**, *7*, 10424–10432.
- (14) Zhang, B.; Zhang, L.; Deng, W.; Jin, L.; Chun, F.; Pan, H.; Gu, B.; Zhang, H.; Lv, Z.; Yang, W.; Wang, Z. L. Self-Powered Acceleration Sensor Based on Liquid Metal Triboelectric Nanogenerator for Vibration Monitoring. *ACS Nano* **2017**, *11*, 7440–7446.
- (15) Wu, C.; Liu, R.; Wang, J.; Zi, Y.; Lin, L.; Wang, Z. L. A Spring-Based Resonance Coupling for Hugely Enhancing the Performance of Triboelectric Nanogenerators for Harvesting Low-Frequency Vibration Energy. *Nano Energy* **2017**, *32*, 287–293.
- (16) Xi, Y.; Wang, J.; Zi, Y.; Li, X.; Han, C.; Cao, X.; Hu, C.; Wang, Z. High Efficient Harvesting of Underwater Ultrasonic Wave Energy by Triboelectric Nanogenerator. *Nano Energy* **2017**, *38*, 101–108.
- (17) Wang, X.; Niu, S.; Yi, F.; Yin, Y.; Hao, C.; Dai, K.; Zhang, Y.; You, Z.; Wang, Z. L. Harvesting Ambient Vibration Energy over a Wide Frequency Range for Self-Powered Electronics. *ACS Nano* **2017**, *11*, 1728–1735.
- (18) Wang, P.; Liu, R.; Ding, W.; Zhang, P.; Pan, L.; Dai, G.; Zou, H.; Dong, K.; Xu, C.; Wang, Z. L. Complementary Electromagnetic-Triboelectric Active Sensor for Detecting Multiple Mechanical Triggering. *Adv. Funct. Mater.* **2018**, *28*, 1705808.

- (19) Wang, X. F.; Niu, S. M.; Yin, Y. J.; Yi, F.; You, Z.; Wang, Z. L. Triboelectric Nanogenerator Based on Fully Enclosed Rolling Spherical Structure for Harvesting Low-Frequency Water Wave Energy. *Adv. Energy Mater.* **2015**, *5*, 1501467.
- (20) Zhu, D.; Tudor, M. J.; Beeby, S. P. Strategies for Increasing the Operating Frequency Range of Vibration Energy Harvesters: A Review. *Meas. Sci. Technol.* **2010**, *21*, No. 022001.
- (21) Cui, S.; Zheng, Y.; Liang, J.; Wang, D. Conducting Polymer PPY Nanowire-Based Triboelectric Nanogenerator and Its Application for Self-Powered Electrochemical Cathodic Protection. *Chem. Sci.* **2016**, *7*, 6477–6483.
- (22) Tang, W.; Han, Y.; Han, C. B.; Gao, C. Z.; Cao, X.; Wang, Z. L. Self-Powered Water Splitting Using Flowing Kinetic Energy. *Adv. Mater.* **2015**, *27*, 272–276.
- (23) Yeh, M.-H.; Guo, H.; Lin, L.; Wen, Z.; Li, Z.; Hu, C.; Wang, Z. L. Rolling Friction Enhanced Free-Standing Triboelectric Nanogenerators and Their Applications in Self-Powered Electrochemical Recovery Systems. *Adv. Funct. Mater.* **2016**, *26*, 1054–1062.
- (24) Yang, X. H.; Zhu, G.; Wang, S. H.; Zhang, R.; Lin, L.; Wu, W. Z.; Wang, Z. L. A Self-Powered Electrochromic Device Driven by a Nanogenerator. *Energy Environ. Sci.* **2012**, *5*, 9462–9466.
- (25) Gao, S.; Zhu, Y.; Chen, Y.; Tian, M.; Yang, Y.; Jiang, T.; Wang, Z. L. Self-Power Electroreduction of N_2 into NH_3 by 3D Printed Triboelectric Nanogenerators. *Mater. Today* **2019**, *28*, 17–24.
- (26) Lin, Z.-H.; Zhu, G.; Zhou, Y. S.; Yang, Y.; Bai, P.; Chen, J.; Wang, Z. L. A Self-Powered Triboelectric Nanosensor for Mercury Ion Detection. *Angew. Chem., Int. Ed.* **2013**, *S2*, 5065–5069.
- (27) Li, C.; Yin, Y.; Wang, B.; Zhou, T.; Wang, J.; Luo, J.; Tang, W.; Cao, R.; Yuan, Z.; Li, N.; Du, X.; Wang, C.; Zhao, S.; Liu, Y.; Wang, Z. L. Self-Powered Electrospinning System Driven by a Triboelectric Nanogenerator. *ACS Nano* **2017**, *11*, 10439–10445.
- (28) Liu, G.; Guo, H.; Xu, S.; Hu, C.; Wang, Z. L. Oblate Spheroidal Triboelectric Nanogenerator for All-Weather Blue Energy Harvesting. *Adv. Energy Mater.* **2019**, *9*, 1900801.
- (29) Wang, Z. L. Triboelectric Nanogenerators as New Energy Technology and Self-Powered Sensors - Principles, Problems and Perspectives. *Faraday Discuss.* **2014**, *176*, 447–458.
- (30) Wang, Z. L. On Maxwell's Displacement Current for Energy and Sensors: The Origin of Nanogenerators. *Mater. Today* **2017**, *20*, 74–82.
- (31) Niu, S.; Wang, Z. L. Theoretical Systems of Triboelectric Nanogenerators. *Nano Energy* **2015**, *14*, 161–192.
- (32) Niu, S.; Wang, S.; Lin, L.; Liu, Y.; Zhou, Y. S.; Hu, Y.; Wang, Z. L. Theoretical Study of Contact-Mode Triboelectric Nanogenerators as an Effective Power Source. *Energy Environ. Sci.* **2013**, *6*, 3576–3586.
- (33) Wen, X.; Yang, W.; Jing, Q.; Wang, Z. L. Harvesting Broadband Kinetic Impact Energy from Mechanical Triggering/Vibration and Water Waves. *ACS Nano* **2014**, *8*, 7405–7412.
- (34) Xu, M.; Wang, P.; Wang, Y.-C.; Zhang, S. L.; Wang, A. C.; Zhang, C.; Wang, Z.; Pan, X.; Wang, Z. L. A Soft and Robust Spring Based Triboelectric Nanogenerator for Harvesting Arbitrary Directional Vibration Energy and Self-Powered Vibration Sensing. *Adv. Energy Mater.* **2018**, *8*, 1702432.
- (35) Yang, W.; Chen, J.; Zhu, G.; Wen, X.; Bai, P.; Su, Y.; Lin, Y.; Wang, Z. Harvesting Vibration Energy by a Triple-Cantilever Based Triboelectric Nanogenerator. *Nano Res.* **2013**, *6*, 880–886.
- (36) Pan, L.; Wang, J.; Wang, P.; Gao, R.; Wang, Y.-C.; Zhang, X.; Zou, J.-J.; Wang, Z. L. Liquid-FEP-Based U-Tube Triboelectric Nanogenerator for Harvesting Water-Wave Energy. *Nano Res.* **2018**, *11*, 4062–4073.
- (37) Lee, K. Y.; Chun, J.; Lee, J. H.; Kim, K. N.; Kang, N. R.; Kim, J. Y.; Kim, M. H.; Shin, K. S.; Gupta, M. K.; Baik, J. M.; Kim, S. W. Hydrophobic Sponge Structure-Based Triboelectric Nanogenerator. *Adv. Mater.* **2014**, *26*, 5037–5042.
- (38) Sun, K.; Jing, Y.; Li, C.; Zhang, X.; Aguinaldo, R.; Kargar, A.; Madsen, K.; Banu, K.; Zhou, Y.; Bando, Y.; Liu, Z.; Wang, D. 3D Branched Nanowire Heterojunction Photoelectrodes for High-Efficiency Solar Water Splitting and H_2 Generation. *Nanoscale* **2012**, *4*, 1515–1521.
- (39) Parthiban, G. T.; Parthiban, T.; Ravi, R.; Saraswathy, V.; Palaniswamy, N.; Sivan, V. Cathodic Protection of Steel in Concrete Using Magnesium Alloy Anode. *Corros. Sci.* **2008**, *50*, 3329–3335.